Physics Letters B 684 (2010) 11–16

Contents lists available at ScienceDirect

Physics Letters B

www.elsevier.com/locate/physletb

Measurement of the invariant mass distributions for the $pp \to pp\eta'$ reaction at excess energy of $Q = 16.4$ MeV

P. Klaja [a,b,c,*], P. Moskal [a,b], E. Czerwiński [a,b], R. Czyżykiewicz [a], A. Deloff [d], D. Gil [a], D. Grzonka [b], L. Jarczyk [a], B. Kamys [a], A. Khoukaz [e], J. Klaja [a,b], K. Nakayama [f], W. Oelert [b], J. Ritman [b], T. Sefzick [b], M. Siemaszko [g], M. Silarski [a], J. Smyrski [a], A. Täschner [e], M. Wolke [b], J. Zdebik [a], M. Zieliński [a,b], W. Zipper [g]

[a] Institute of Physics, Jagellonian University, PL-30-059 Cracow, Poland
[b] Institut für Kernphysik, Forschungszentrum Jülich, D-52425 Jülich, Germany
[c] Physikalisches Institut, Universität Erlangen–Nürnberg, D-91058 Erlangen, Germany
[d] Institute for Nuclear Studies, PL-00-681 Warsaw, Poland
[e] Institut für Kernphysik, Westfälische Wilhelms–Universität, D-48149 Münster, Germany
[f] Department of Physics, University of Georgia, GA-30602 Athens, USA
[g] Institute of Physics, University of Silesia, PL-40-007 Katowice, Poland

ARTICLE INFO

Article history:
Received 20 October 2009
Received in revised form 15 December 2009
Accepted 22 December 2009
Available online 6 January 2010
Editor: D.F. Geesaman

Keywords:
Pseudoscalar mesons
Differential distributions
Near threshold meson production
Interaction

ABSTRACT

The proton–proton and proton–η' invariant mass distributions have been determined for the $pp \to pp\eta'$ reaction at an excess energy of $Q = 16.4$ MeV. The measurement was carried out using the COSY-11 detector setup and the proton beam of the cooler synchrotron COSY. The shapes of the determined invariant mass distributions are similar to those of the $pp \to pp\eta$ reaction and reveal an enhancement for large relative proton–proton momenta. This result, together with the fact that the proton–η interaction is much stronger that the proton–η' interaction, excludes the hypothesis that the observed enhancement is caused by the interaction between the proton and the meson.

1. Introduction

The understanding of the meson–nucleon interaction as well as studies of meson structure and production mechanisms constitute one of the basic issues of the contemporary hadron physics. The η and η' mesons constitute a mixture of the SU(3) singlet and octet states with almost the same relative contributions of various quark flavors. Nevertheless, they have unexpectedly different properties, e.g. as regards the mass [1], branching ratios [2,3] or production cross sections [4]. These differences indicate that also the interaction of η and η' mesons with nucleons may be different.

Up to now, the proton–η interaction was studied intensively but still rather large range of values of the scattering length is reported depending on the analysis method [5]. The proton–η' interaction is much less known. It is only qualitatively estimated (based on the $pp \to pp\eta'$ excitation function) to be much weaker than for the proton–η system [6]. In principle, studies of $pp \to pp$meson reactions permit information about the proton–meson interaction to be gained not only from the shape of the excitation function but also from differential distributions of proton–proton and proton–meson invariant masses. Therefore, in order to investigate the proton–η interaction the COSY-11 collaboration performed a measurement [4] of the proton–η and proton–proton invariant mass distributions close to the threshold at $Q = 15.5$ MeV, where the outgoing particles possess small relative velocities. Indeed a large enhancement in the region of small proton–η and large proton–proton relative momenta was observed.[1] However, the observed effect cannot be univocally assigned to the influence of the proton–η interaction in the final state [8,9], since it can also be explained by the admixture of higher partial waves in the proton–proton

* Corresponding author at: Institut für Kernphysik, Forschungszentrum Jülich, D-52425 Jülich, Germany.
E-mail addresses: p.klaja@fz-juelich.de (P. Klaja), p.moskal@fz-juelich.de (P. Moskal).

[1] The same enhancement was also seen in independent measurements by the COSY-TOF group [7].

0370-2693/$ – see front matter
doi:10.1016/j.physletb.2009.12.056

system [10], or by the energy dependence of the production amplitude [11,12].

The endeavor to explain the origin of the observed enhancement motivated the measurement of the proton–proton and proton–η' invariant mass distributions for the $pp \to pp\eta'$ reaction presented in this Letter.

If the enhancement observed in the proton–proton invariant mass distributions for the $pp \to pp\eta$ reaction would be due to the proton–η interaction then it is expected to be significantly lower for the $pp \to pp\eta'$ reaction since the proton–η interaction is stronger than the proton–η' [6].

In order to make a model independent comparison of the spectra in the $pp\eta$ and $pp\eta'$ systems we performed a measurement of the $pp \to pp\eta'$ reaction, nominally at the same excess energy as previously measured for the $pp \to pp\eta$ reaction. Invariant mass spectra determined at the same excess energies allow for the comparison without a need for a correction of kinematical factors in the outgoing system.

It is important to stress that the invariant mass distributions for the $pp \to pp\eta'$ reaction have not been measured so far. This is because the total cross section for the η' meson production in hadron collisions is by more than a factor of 30 smaller than the one for the η meson at the same excess energy and additionally the total cross section for the production of the multi-pion background grows by three orders of magnitude when the beam energy increases from the η to the η' production threshold [13]. A determination of the invariant mass spectra reported in this Letter was made possible due to stochastic cooling of the proton beam of the COSY synchrotron [14–17] and the good momentum resolution ($\sigma = 4$ MeV/c) [4] achieved with the COSY-11 detector setup designed especially for measurements near the kinematical threshold. Sufficient statistics were collected to allow the background to be subtracted from the invariant mass distributions.

Detailed description of the COSY-11 method used for the $pp \to pp\eta'$ reaction measurements can be found in [18–20], therefore, here we concentrate on the background subtraction procedure crucial for the determination of invariant mass distributions.

2. Experiment and data analysis

The measurement of the $pp \to pp\eta'$ reaction was conducted using the cooler synchrotron COSY [14] and the COSY-11 detector setup [21–23] at the proton beam momentum of $p_B = 3.260$ MeV/c, which corresponds to an excess energy of $Q = 16.4$ MeV. It was based on the registration of the two outgoing protons and reconstruction of their momenta. The η' meson is identified using the missing mass technique.

Fig. 1 illustrates a schematic view of the COSY-11 apparatus with a topology of the $pp \to ppX$ reaction. Two outgoing protons possessing smaller momenta than the beam momentum are bent in the dipole magnetic field towards the detector system leaving the vacuum chamber through the exit window. Afterwards, they are detected in the two drift chambers, D1 and D2, in the scintillator hodoscopes S1 and S2, and in the scintillator wall S3. The target[2] used during the experiment, was realized as a beam of H_2 molecules grouped inside clusters of up to about 10^6 atoms. The average density of the target was around $5 \cdot 10^{13}$ atoms/cm^2 [24]. It was installed in front of the dipole magnet as it can be seen schematically in Fig. 1.

In order to determine the absolute values of the differential cross sections, the time integrated luminosity (L) has been established by the concurrent measurement of the angular distribution

[2] The H_2 cluster target specifications are described in references [22,24].

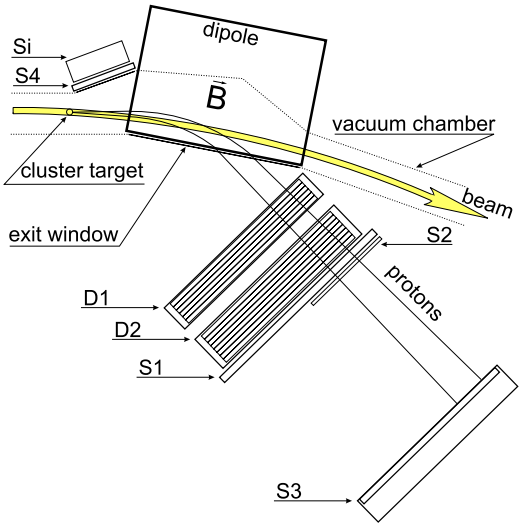

Fig. 1. Schematic view of the COSY-11 detector facility [21]. Protons originating from the $pp \to ppX$ reaction are bent in the dipole magnetic field, and leave the vacuum chamber through the exit window. Afterwards they are detected in the two drift chambers D1 and D2, in the scintillator hodoscopes S1 and S2, and in the scintillator wall S3. The scintillation detector S4 and the silicon pad detector Si are used in coincidence with the D1, D2 and S1 detectors for the registration of the elastically scattered protons.

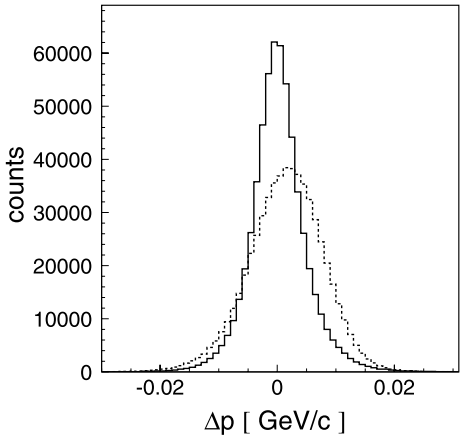

Fig. 2. Spectrum of the difference between the simulated and reconstructed proton momentum. The dashed line denotes the spectrum before kinematical fit and the solid line corresponds to the situation after the fitting procedure.

of the elastically scattered protons [25]. The extracted value of the integrated luminosity amounts to $L = (5.859 \pm 0.055)$ pb^{-1} [26].

In order to search for small effects like proton–meson interaction it is of importance to account for smearing of the measured distributions due to the finite resolution of the detector system, which may alter the shape of the spectrum especially close to the kinematical limit. Therefore, as has been done previously in the analysis of the $pp \to pp\eta$ reaction [4], a kinematical fitting of the data has been performed [26] in order to improve resolution. To this end, the momenta of the protons were varied demanding that the missing mass of the unregistered particle equals the known mass of the η' meson exactly. Furthermore, as a result of the fit, only those proton momentum vectors which were closest to the vectors determined from the experiment have been chosen. The inverse of the covariance matrix was used as a metric for the distance calculation. The kinematical fit improves the resolution by a factor of 1.5, as can be seen in Fig. 2. After the kinematical fit each event can be characterized by both: experimentally deter-

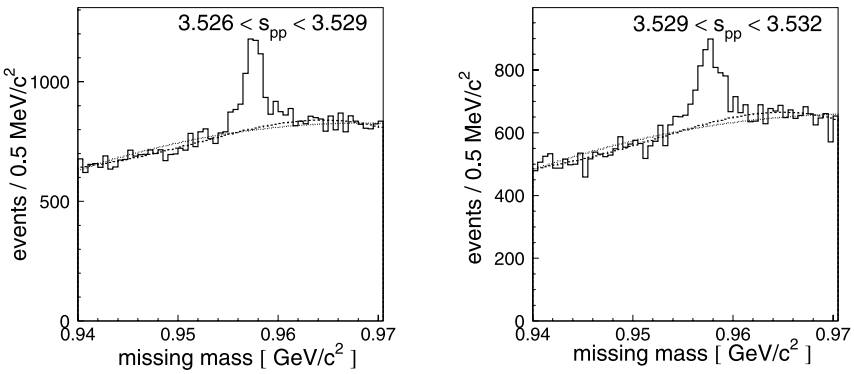

Fig. 3. Examples of experimental missing mass spectra for two intervals of s_{pp} as indicated in the figure. The dotted lines indicate second order polynomials and the dashed lines show the sum of two Gaussian distributions.

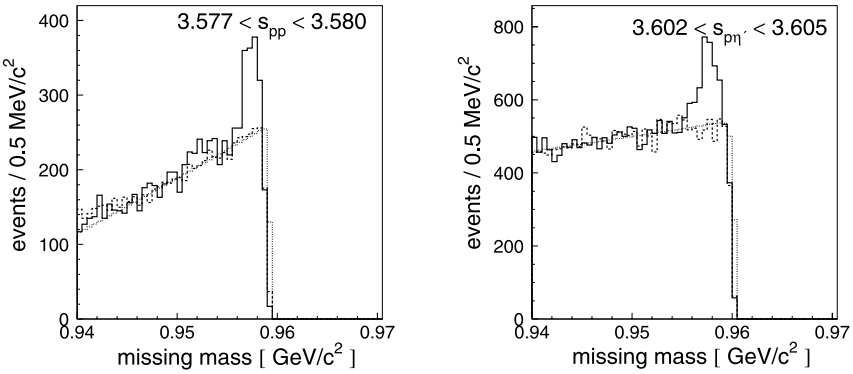

Fig. 4. Examples of measured missing mass spectra for the $pp \to ppX$ reaction (solid lines) with superimposed Monte Carlo simulations of multi-pionic background (dashed lines). The missing mass spectra are presented for squared invariant proton–proton mass $s_{pp} \in [3.577; 3.580]$ GeV$^2/c^4$ (left) and squared invariant proton–η' mass $s_{p\eta'} \in [3.602; 3.605]$ GeV$^2/c^4$ (right). The dotted lines in both panels correspond to the fit of Eq. (1).

mined momentum vectors and kinematically fitted momenta. In the subsequent analysis the fitted momenta were used to group events into s_{pp} and $s_{p\eta'}$ intervals and then in order to subtract the background, for each group separately, a missing mass spectrum was determined from experimental momentum vectors. The available range of s_{pp} and $s_{p\eta'}$ was divided into 22 bins. The width of the bins (0.003 GeV$^2/c^4$) was chosen as a compromise between statistics and the experimental resolution. Then, for each bin, the missing mass spectrum was reconstructed and the number of the $pp \to pp\eta'$ events was calculated separately for each interval of s_{pp}, $s_{p\eta'}$.

In Fig. 3, examples of missing mass spectra for two intervals of the invariant proton–proton mass are presented. A clear signal from the η' meson production is seen on top of a continuous spectrum from the multi pion background. A smooth behavior of the background allows one to interpolate its shape under the η' peak with polynomial functions that match the data below and above the peak. The smooth behavior of the multi-pion background in the peak region was verified by Monte Carlo simulations [26]. In both panels of Fig. 3 the dotted lines correspond to the result of the fit of the second order polynomial. An equally good approximation of the background was also achieved by a fit of the sum of two Gaussian distributions [26]. The parameterizations were performed in the entire range of missing mass outside of the $pp \to pp\eta'$ signal, and obviously reproduce the background very well.

The situation is more complicated for these missing mass spectra when the signal is close to the kinematical limit (see Fig. 4). In this case the shape of the background on the right side of the peak cannot be easily predicted. Such spectra are obtained for kinematical regions of higher squared invariant proton–proton masses and relatively low squared invariant proton–η' masses. In order to describe the shape of the background in these regions, the $pp \to pp2\pi\eta$, $pp \to pp3\pi$ and $pp \to pp4\pi$ reactions[3] have been generated and the simulated events were analyzed in the same way as for the experimental data. The result of these simulations (dashed lines) is compared to the experimental data in Fig. 4. The simulations of the different reaction channels were performed with a distribution based on an equal population of phase space including the proton–proton final state interaction [6,27]. A linear sum of the simulated missing mass spectra was matched to the data with the relative magnitudes as the only free parameters. In both examples, simulations are in a good agreement with the experimental background distributions below the η' peak. Moreover the behavior of the simulated background matches the kinematical limit of the missing mass distributions.

For the dynamics of the pion production, it had been assumed that pions are produced uniformly over the available phase space. As described in reference [27] the shape of the missing mass spectrum does not change significantly at the edge of the kinematical limit if one assumes resonant or direct pion production.

In order to increase the confidence in the estimation of the background behavior near the kinematical boundary and to estimate the systematic uncertainties due to the choice of the background parameterizations, these distributions were described in an

[3] These reaction channels were chosen as a representation of the possible multi-pion production background, since contribution from the $pp \to pp5\pi$, 6π, 7π reactions can be neglected [18] and the missing mass spectrum from 2π has a similar shape as those for 3π and 4π in the relevant kinematical region.

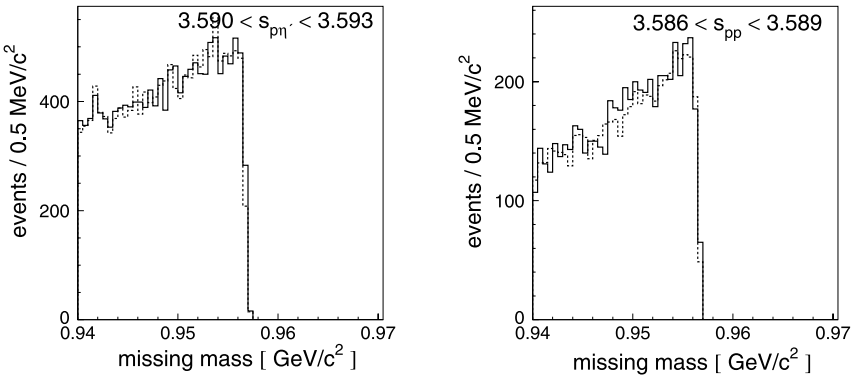

Fig. 5. Missing mass spectra for low values of $s_{p\eta'} \in [3.590; 3.593]$ GeV$^2/c^4$ (left) and high values of $s_{pp} \in [3.586; 3.589]$ GeV$^2/c^4$ (right). The dashed lines correspond to a linear sum of the simulated $pp \to pp2\pi\eta$, $pp \to pp3\pi$ and $pp \to pp4\pi$ reactions (solid lines) using only the magnitudes as free parameters.

independent way with a second order polynomial divided by the Fermi function for the description of the rapid slope at the end of the distributions. To this end, the following formula was applied:

$$F(mm, a, b, c, d, g) = \left(a + b \cdot mm + c \cdot mm^2\right) / \left(1 + e^{(mm-d)/g}\right), \quad (1)$$

where a, b, c, d and g are free parameters.

The results are presented in Fig. 4 as dotted lines. It is seen that under the η' peak the result of Eq. (1) agrees well with the background determined from the simulations and that both reproduce the shape of the slope quite well.

A further check of the background was performed by extracting the missing mass distributions for regions of the squared invariant masses of proton–proton and proton–meson where the η' is not produced. The resulting missing mass distributions are shown in Fig. 5 and represent the regions of low squared invariant masses of the proton–meson subsystem (left) and high squared invariant masses of the proton–proton subsystem (right). For such values of s_{pp} or $s_{p\eta'}$ the production of the η' meson is not kinematically allowed because $s_{p\eta'} < (m_p + m_{\eta'})^2$ and s_{pp} is too large leaving insufficient energy to create the η' meson. The simulations reproduce the background very well as one can see in Fig. 5.

The main contribution to the systematic uncertainty of the determined differential cross sections comes from the uncertainty of the estimation of the yield of the η' events which, in turn, is due to the assumption of the shape of the background. In order to estimate these errors, the numbers of background events extracted under the two different assumptions were compared. For the missing mass spectra with the signal far from the kinematical limit, the background determined by Gaussian distributions was compared to the background estimated by a second order polynomial. For the spectra close to the kinematical limit, the background determination by Monte Carlo simulations was compared to a second order polynomial divided by the Fermi distribution. The uncertainty of the background estimation constitutes the main contribution to the systematic error of the differential cross sections. The differences in the number of background events obtained by applying the above described different fit procedures are below 3% of the background value, which corresponds to about 20% of the signal, as can be seen for instance in Fig. 4.

Finally, the measured distributions were corrected for the acceptance according to the method described elsewhere [4]. Here, it is important to stress that at the beam momentum of $p_B = 3.260$ GeV/c the COSY-11 acceptance for the $pp \to pp\eta'$ reaction is finite over the entire area of the s_{pp} vs. $s_{p\eta'}$ Dalitz plot. This is shown in Fig. 6, where one can see that the full phase space for the $pp \to pp\eta'$ reaction is covered.

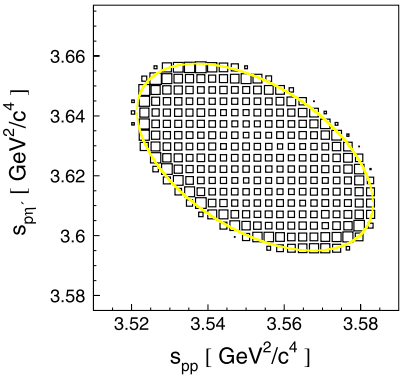

Fig. 6. COSY-11 detection acceptance as a function of s_{pp} and $s_{p\eta'}$ squared invariant masses. Dalitz plot distribution was reconstructed from the events accepted by the COSY-11 detector setup.

3. Results

A comparison of the s_{pp} and $\sqrt{s_{p-\text{meson}}}$ distributions between the $pp \to pp\eta'$ and the $pp \to pp\eta$ reactions is presented in Fig. 7. For the proton–meson system the comparison was performed for the kinetic energy $(\sqrt{s_{p-\text{meson}}} - m_p - m_{\text{meson}})$ and not as a function of $s_{p-\text{meson}}$ because the range of the $s_{p\eta}$ and $s_{p\eta'}$ are different due to the different masses of the η and η' mesons. But the range of $(\sqrt{s_{p-\text{meson}}} - m_p - m_{\text{meson}})$ is the same since the measurements for the η and η' production were performed at about the same excess energy.[4]

In both panels it is seen that the shape of the distribution for the $pp \to pp\eta$ measurement (open squares) is in agreement with that for the $pp \to pp\eta'$ reaction (closed squares) within the error bars, thus, showing the same enhancement in the region of large proton–proton invariant mass. Therefore, if the η'–proton interaction is indeed much smaller than the η–proton as inferred from the excitation function [4,6], then, one would have observed a significantly smaller enhancement in the case of the η' meson. Hence, the spectra presented here tend to exclude the hypothesis that the enhancement is due to the meson–proton interaction.

The absolute values of the cross section for the $pp \to pp\eta'$ reaction determined as a function of s_{pp} and $s_{p\eta'}$ are given in

[4] The nominal beam energy corresponds to an excess energy of $Q = 15.5$ MeV, consistent with the data collected for the $pp \to pp\eta$ reaction. However, the real value was determined to be 16.4 MeV [26]. This difference is well within the precision of the absolute beam momentum adjustment of the COSY synchrotron amounting to about $\delta p/p = 10^{-3}$ [15] which corresponds to ~ 1 MeV uncertainty in Q.

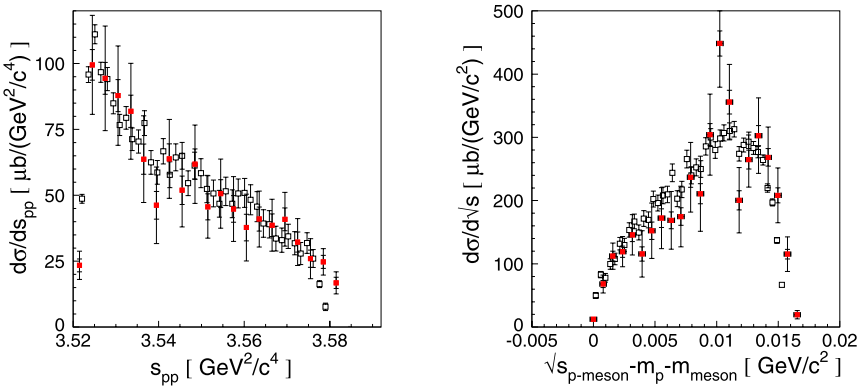

Fig. 7. Comparison of the proton–proton invariant mass squared distributions (s_{pp}) (left) and of proton–meson kinetic energy ($\sqrt{s_{p-\mathrm{meson}}} - m_p - m_{\mathrm{meson}}$) (right). The distributions for the $pp \to pp\eta'$ reaction (filled squares) were normalized to the same total cross section as the $pp \to pp\eta$ reaction (open squares). Statistical and systematic errors were separated by horizontal dashes.

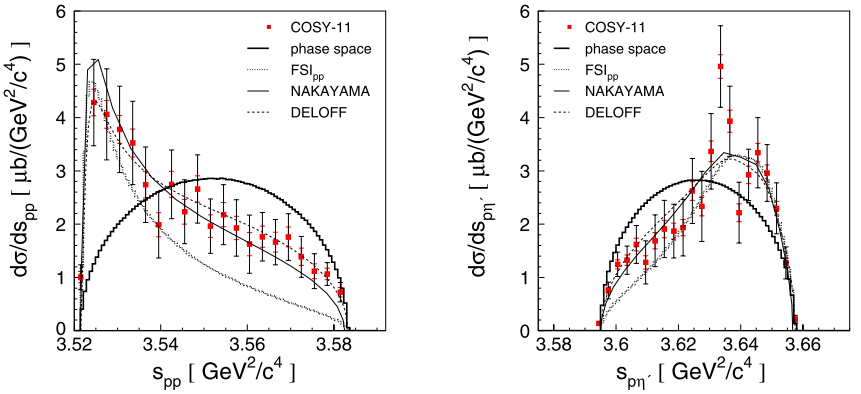

Fig. 8. Distributions of the squared proton–proton (s_{pp}) and proton–η' ($s_{p\eta'}$) invariant masses, for the $pp \to pp\eta'$ reaction at the excess energy of $Q = 16.4$ MeV. The experimental data (closed squares) are compared to the expectation under the assumption of a homogeneously populated phase space (thick solid lines) and the integrals of the phase space weighted by the proton–proton scattering amplitude – FSI_{pp} (dotted histograms). The solid and dashed lines correspond to calculations when taking into account contributions from higher partial waves and allowing for a linear energy dependence of the ${}^3P_0 \to {}^1S_0 s$ partial wave amplitude, respectively.

Table 1
Differential cross section as a function of the squared invariant mass of the proton–proton system, for the $pp \to pp\eta'$ reaction at $Q = 16.4$ MeV.

s_{pp} [GeV$^2/c^4$]	$\frac{d\sigma}{ds_{pp}}$ [μb/GeV$^2/c^4$]
3.5215	$1.01 \pm 0.11_{stat} \pm 0.12_{sys}$
3.5245	$4.28 \pm 0.25_{stat} \pm 0.56_{sys}$
3.5275	$4.06 \pm 0.26_{stat} \pm 0.59_{sys}$
3.5305	$3.78 \pm 0.26_{stat} \pm 0.55_{sys}$
3.5335	$3.52 \pm 0.26_{stat} \pm 0.52_{sys}$
3.5365	$2.74 \pm 0.25_{stat} \pm 0.46_{sys}$
3.5395	$1.99 \pm 0.23_{stat} \pm 0.40_{sys}$
3.5425	$2.75 \pm 0.25_{stat} \pm 0.40_{sys}$
3.5455	$2.23 \pm 0.23_{stat} \pm 0.37_{sys}$
3.5485	$2.66 \pm 0.25_{stat} \pm 0.39_{sys}$
3.5515	$1.96 \pm 0.21_{stat} \pm 0.30_{sys}$
3.5545	$2.18 \pm 0.23_{stat} \pm 0.34_{sys}$
3.5575	$1.93 \pm 0.22_{stat} \pm 0.31_{sys}$
3.5605	$1.62 \pm 0.22_{stat} \pm 0.33_{sys}$
3.5635	$1.76 \pm 0.20_{stat} \pm 0.26_{sys}$
3.5665	$1.66 \pm 0.19_{stat} \pm 0.24_{sys}$
3.5695	$1.76 \pm 0.19_{stat} \pm 0.26_{sys}$
3.5725	$1.39 \pm 0.16_{stat} \pm 0.22_{sys}$
3.5755	$1.12 \pm 0.14_{stat} \pm 0.19_{sys}$
3.5785	$1.07 \pm 0.11_{stat} \pm 0.11_{sys}$
3.5815	$0.72 \pm 0.09_{stat} \pm 0.09_{sys}$
3.5845	$0.013 \pm 0.004_{stat} \pm 0.002_{sys}$

Table 2
Differential cross section as a function of the squared invariant mass of the proton–η' system, for the $pp \to pp\eta'$ reaction at $Q = 16.4$ MeV.

$s_{p\eta'}$ [GeV$^2/c^4$]	$\frac{d\sigma}{ds_{p\eta'}}$ [μb/GeV$^2/c^4$]
3.5945	$0.14 \pm 0.02_{stat} \pm 0.02_{sys}$
3.5975	$0.76 \pm 0.06_{stat} \pm 0.09_{sys}$
3.6005	$1.25 \pm 0.09_{stat} \pm 0.14_{sys}$
3.6035	$1.32 \pm 0.10_{stat} \pm 0.17_{sys}$
3.6065	$1.62 \pm 0.12_{stat} \pm 0.24_{sys}$
3.6095	$1.28 \pm 0.13_{stat} \pm 0.28_{sys}$
3.6125	$1.69 \pm 0.15_{stat} \pm 0.33_{sys}$
3.6155	$1.91 \pm 0.16_{stat} \pm 0.37_{sys}$
3.6185	$1.87 \pm 0.15_{stat} \pm 0.36_{sys}$
3.6215	$1.94 \pm 0.15_{stat} \pm 0.38_{sys}$
3.6245	$2.62 \pm 0.18_{stat} \pm 0.44_{sys}$
3.6275	$2.33 \pm 0.18_{stat} \pm 0.48_{sys}$
3.6305	$3.37 \pm 0.19_{stat} \pm 0.51_{sys}$
3.6335	$4.96 \pm 0.22_{stat} \pm 0.54_{sys}$
3.6365	$3.93 \pm 0.21_{stat} \pm 0.45_{sys}$
3.6395	$2.21 \pm 0.17_{stat} \pm 0.40_{sys}$
3.6425	$2.93 \pm 0.16_{stat} \pm 0.32_{sys}$
3.6455	$3.34 \pm 0.18_{stat} \pm 0.48_{sys}$
3.6485	$2.96 \pm 0.15_{stat} \pm 0.38_{sys}$
3.6515	$2.30 \pm 0.13_{stat} \pm 0.35_{sys}$
3.6545	$1.27 \pm 0.08_{stat} \pm 0.22_{sys}$
3.6575	$0.22 \pm 0.03_{stat} \pm 0.04_{sys}$

Tables 1 and 2, and are shown in Fig. 8. The determined distributions differ significantly from the predictions based on the homogeneous phase space population (thick solid line). Also, the results of calculations including the FSI_{pp} (dotted line) do not describe the data underestimating the cross sections at large values of s_{pp} and low values of $s_{p\eta}$. Similarly to the case of η meson,

a better agreement with the experimental data can be achieved when taking into account contributions from higher partial waves. The calculations depicted as solid lines result from a combined analysis (based on the effective Lagrangian approach) of the production of η and η' mesons in photo- and hadro-induced reactions [10,28–30]. Since the calculation is done in the plane-wave basis, not only the ${}^3P_0 \to {}^1S_0 s$ but also the ${}^1S_0 \to {}^3P_0 s$ (and all the higher partial-waves) transition[5] contributes at the excess energy of 16.4 MeV.

On the other hand, one can explain the enhancement seen in the distributions by an energy dependent production amplitude [11]. The result indicated by the dashed lines was obtained allowing for a linear energy dependence of the ${}^3P_0 \to {}^1S_0 s$ partial wave amplitude and neglecting other partial waves transitions [11]. Also, Ceci et al. [12] have shown recently that the discussed enhancement in the invariant mass spectra can be well described by the energy dependence of the production amplitude when the negative interference between the π and the η meson exchange amplitudes is assumed.

Within the statistical and systematic error bars both model of Nakayama et al. [10] and of Deloff [11] describe the data well although they differ slightly in the predicted shapes. Taking into account statistical uncertainties only, one obtains $\chi^2 = 2.1$ and $\chi^2 = 4.7$ for the comparison of the dashed line and solid line to the data, respectively. This indicates that perhaps, not only higher partial waves but also the energy dependence of the production amplitude should be taken into account.

4. Summary

Using the COSY-11 detector setup and the proton beam of the cooler synchrotron COSY the proton–proton and proton–η' invariant mass distributions have been determined for the $pp \to pp\eta'$ reaction at an excess energy of $Q = 16.4$ MeV.

Similar to the earlier observation for the η meson production the measured differential cross section distributions (s_{pp} and $s_{p\eta'}$) for the $pp \to pp\eta'$ reaction at $Q = 16.4$ MeV strongly deviate from the predictions based on a homogeneous population of events over the allowed phase space. Also, the inclusion of the proton–proton final state interaction is not sufficient to explain the enhancement seen in the range of large s_{pp} values.

Within the achieved uncertainties, the shape of the proton–proton and proton–meson invariant mass distributions determined for theη' meson is essentially the same to that established previously for the η meson.Since the enhancement is similar in both cases, and the strength of proton–$\eta$and proton–η' interaction is different [6,26], one can conclude that the observed enhancementis not caused by a proton–meson interaction.

Finally, calculations assuming a significant contribution of P-wave in thefinal state [10], and models includingenergy dependence of the production amplitude [11,12], reproduce the datawithin error bars equally well.Therefore, on the basis of the presented invariant mass distributions, it is not possibleto disentangle univocally which of the discussed models is more appropriate.As pointed out in [10], future measurements of the spin correlation coefficientsshould help disentangle these two model results in a model independent way.

Acknowledgements

The work was partially supported by the European Community-Research Infrastructure Activity under the FP6 and FP7 programmes (Hadron Physics, RII3-CT-2004-506078, PrimeNet No. 227431), by the Polish Ministry of Science and Higher Education under grants No. 3240/H03/2006/31 and 1202/DFG/2007/03, by the German Research Foundation (DFG), by the FFE grants from the Research Center Jülich, and by the virtual institute "Spin and strong QCD" (VH-VI-231).

References

[1] C. Amsler, et al., Phys. Lett. B 667 (2008) 1.
[2] C.P. Jessop, et al., Phys. Rev. D 58 (1998) 052002.
[3] G. Brandenburg, et al., Phys. Rev. Lett. 75 (1995) 3804.
[4] P. Moskal, et al., Phys. Rev. C 69 (2004) 025203.
[5] A.M. Green, S. Wycech, Phys. Rev. C 71 (2005) 014001.
[6] P. Moskal, et al., Phys. Lett. B 482 (2000) 356.
[7] M. Abdel-Bary, et al., Eur. Phys. J. A 16 (2003) 127.
[8] A. Fix, H. Arenhövel, Phys. Rev. C 69 (2004) 014001.
[9] A. Fix, H. Arenhövel, Nucl. Phys. A 697 (2002) 277.
[10] K. Nakayama, et al., Phys. Rev. C 68 (2003) 045201.
[11] A. Deloff, Phys. Rev. C 69 (2004) 035206.
[12] S. Ceci, A. Švarc, B. Zauner, Acta Phys. Pol. B Suppl. 2 (2009) 157.
[13] M. Zieliński, Diploma Thesis, e-print: arXiv:hep-ex/0807.0576.
[14] R. Maier, Nucl. Instr. Meth. A 390 (1997) 1.
[15] D. Prasuhn, et al., Nucl. Instr. Meth. A 441 (2000) 167.
[16] H. Stockhorst, et al., IKP Annu. Rep. (1997) 160.
[17] H. Stockhorst, Matter Mater. 11 (2002) 176.
[18] P. Moskal, et al., Phys. Rev. Lett. 80 (1998) 3202.
[19] P. Moskal, et al., Phys. Lett. B 474 (2000) 416.
[20] A. Khoukaz, et al., Eur. Phys. J. A 20 (2004) 345.
[21] S. Brauksiepe, et al., Nucl. Instr. Meth. A 376 (1996) 397.
[22] H. Dombrowski, et al., Nucl. Instr. Meth. A 386 (1997) 228.
[23] P. Klaja, et al., AIP Conf. Proc. 796 (2005) 160.
[24] A. Khoukaz, et al., Eur. Phys. J. D 5 (1999) 275.
[25] P. Moskal, et al., Nucl. Instr. Meth. A 466 (2001) 448.
[26] P. Klaja, PhD thesis, e-print: arXiv:0907.1491.
[27] P. Moskal, et al., J. Phys. G 32 (2006) 629.
[28] K. Nakayama, Y. Oh, H. Haberzettl, Acta Phys. Pol. B Suppl. 2 (2009) 23.
[29] K. Nakayama, H. Haberzettl, Phys. Rev. C 69 (2004) 065212.
[30] K. Nakayama, Y. Oh, H. Haberzettl, e-print: arXiv:hep-ph/0803.3169.
[31] H.O. Meyer, et al., Phys. Rev. C 63 (2001) 064002.

[5] The transition between angular momentum combinations of the initial and final states are described according to the conventional notation [31] in the following way:

$$^{2S^i+1}L^i_J \to {}^{2S+1}L_J, l, \qquad (2)$$

where superscript "i" indicates the initial state quantities, S denotes the total spin of nucleons, and J stands for the overall angular momentum of the system. L and l denote the relative angular momentum of nucleon–nucleon pair and of the meson relative to the NN system, respectively.